Scattering-based sensitivity kernels for time-lapse differential-waveform inversion

Daniel Leal Macedo* (CEP/UNICAMP & INCT-GP), Ivan Vasconcelos (Schlumberger Gould Research) and Joerg Schleicher (DMA/IMECC/UNICAMP and INCT-GP/CNPQ/MCT)

Abstract

Time-lapse seismic surveys have become a powerful reservoir monitoring tool. The basic approach in time-lapse surveys is to image the changes in the reservoir by subtracting separated-in-time seismic images of the reservoir. Recently FWI has been used as an alternative time-lapse monitoring tool. However, in practice nonlinear gradient-based FWI is limited due to its notorious sensitivity to the choice of the starting model. Kernel decomposition based on scattering theory allows to break the acoustic-wavefield sensitivity kernels with respect to model parameters into background and singular parts, which should help to address model-convergence issues in FWI. In this work we apply scattering theory to the time-lapse problem, considering the time-lapse change as a perturbation of the singular part of the model. In the framework of time-lapse differential-waveform inversion, and under application of scattering-based decomposition of the sensitivity kernel, we take advantage of the additional illumination of the time-lapse change provided by multiple-scattering phenomena to improve the perturbation estimates from FWI.

Introduction

In the last few years, time-lapse seismic surveys became a powerful tool used to monitor the fluid-flow in a producing reservoir. In general words, such a survey consist in acquiring and analyzing multiple seismic data, repeated at the same site over time in order to look for differences from which one can infer the changes in the reservoir due to production. This is possible because, as fluid saturations and pressures in the reservoir change, the seismic reflection properties change accordingly.

The basic approach in time-lapse surveys is to image the changes in the reservoir by subtracting separated-in-time seismic images of the reservoir. A seismic image contains information on reflections that depends on both the geological structure and its fluid contents. On a single-time images these contributions are coupled and difficult to separate. Assuming that geology is time-invariant during production and that repeatability in the seismic data acquisition is, in some way, assured, the image difference from a time-lapse survey would indicate the changes due only to the fluid-flow since, to first order, the geology part subtracts out since it is time invariant (Lumley, 2001).

Recently FWI has been used as an alternative time-lapse monitoring tool. FWI allows the reconstruction of high-resolution velocity models of the subsurface through the extraction of the full information content of seismic data (Tarantola, 1984; Virieux and Operto, 2009). Since the FWI approach delivers high resolution quantitative images of macro-scale physical parameter, it could be a good candidate for monitoring applications to reconstruct the parameter variation through a time evolution (Asnaashari et al., 2012).

Asnaashari et al. (2012) studied the robustness of three different FWI methods applied to time-lapsed problems: differential method, parallel difference method and the sequential difference method. In the differential method, instead of minimizing the difference between the observed and modeled data, the difference of the differential data between two sets of data is minimized to obtain the time-lapse change estimate (Watanabe et al., 2004). The parallel difference method considers independent inversion of the baseline and monitor data-sets, using a similar starting model (Plessix et al., 2010). The sequential difference method uses the recovered baseline model as a starting model for the monitor data inversion.

While in principle capable of handling all aspects of wave propagation contained in the data, including full nonlinearity, in practice nonlinear gradient-based FWI is limited due to its notorious sensitivity to the choice of the starting model. This is so because, for narrow-offset acquisition of reflection data, the seismic wavefield is rather insensitive to high/intermediate wavelengths.

To help addressing model convergence issues in FWI, we are studying a decomposition based on scattering theory that allows to break the acoustic-wavefield sensitivity kernels (SKs) with respect to model parameters into background and singular parts (Macedo et al., 2012, 2013). We were able to demonstrate that the forward decomposition is successful in bringing out subkernels that unraveled different levels of non-linearity with respect to data and model. This, in turn, could be translated into different levels of interaction between non-, single-, and multiple-scattered information that otherwise would be hidden in the full-wavefield sensitivity kernels. Moreover, we predicted that part of the answer to the problem of lacking low-frequency information on the model should lie in utilizing scattered wavefields, because these travel through the medium long enough to carry this information (see also Snieder et al., 2002).

In this work we apply scattering theory to the time-lapse problem, considering the time-lapse change as

a perturbation of the singular part of the model, i.e., perturbation of the scattering potential. Under the differential method framework, and applying the scattering-based decomposition of the sensitivity kernel, we take advantage of the illumination of the time-lapse change due to multiple-scattering phenomena in order to improve the perturbation estimates from FWI.

Scattering-based sensitivity kernel

The wavefield perturbation due to a medium change, δp, can be evaluated, within Born's approximation assumptions, using the so called secondary or adjoint sources (Tarantola, 1984). Based on scattering theory, we decomposed the full-acoustic-wavefield perturbation δp into 13 components (Figure 1) that reveal different levels of interaction between single and multiple-scattered information within data (Macedo et al., 2012, 2013).

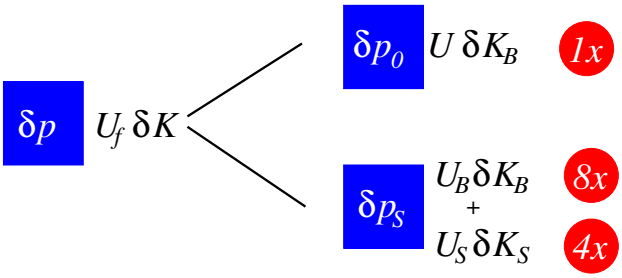

Figure 1: Subkernels obtained from the decomposition considering no perturbation in density. U_f, U, U_B and U_S are Frechet's derivatives, also called sensitivity kernels. The first is the full-wavefield derivative with respect to the full bulk modulus, the second is the reference-wavefield derivative with respect to the background bulk modulus. The last two are scattered-wavefield derivatives with respect to the background and singular part of the bulk modulus respectively.

All components have the same functional structure (time dependency is ommited for simplicity):

$$\delta p_{0/s,\alpha\mathcal{O}\gamma}(x_g;x_s) = \int_{\mathbb{V}} d^3x'\, G_\alpha(x';x_g) * \mathcal{O}\left[p_\gamma(x';x_s)\right] \qquad (1)$$

where G_α is a receiver-side green's function extrapolator; $\mathcal{O}$ a differential operator; p_γ is the source-side wavefield; and $*$ denotes time convolution.

The name of the components of the scattered-wavefield residual follow their physical interpretation according to the possible values α, $\mathcal{O}$ and γ can take (Figure 2). The receiver-wavefield subscript γ is either 0 for the reference wavefield or s for the scattered wavefield. The source-wavefield subscript α can, in addition to 0 and s, also be b, representing the wavefield perturbation due to the background perturbation. The potential index β can take the values B, $\mathcal{B}$, $\mathcal{S}$ and $\mathcal{V}$, representing the background secondary potential, background part of full secondary potential, singular part of full secondary potential, and scattering potential, respectively.

For simplicity, let us analyze the situation without density perturbation. Then, the expression to evaluate the reference- and scattered-wavefield residual is given by

$$\begin{bmatrix} \widehat{\delta p_0} \\ \widehat{\delta p_s} \end{bmatrix} = \begin{bmatrix} U & 0 \\ \sum_i U_{B,i} & \sum_j U_{S,j} \end{bmatrix} \begin{bmatrix} \delta K_B \\ \delta K_S \end{bmatrix}, \qquad (2)$$

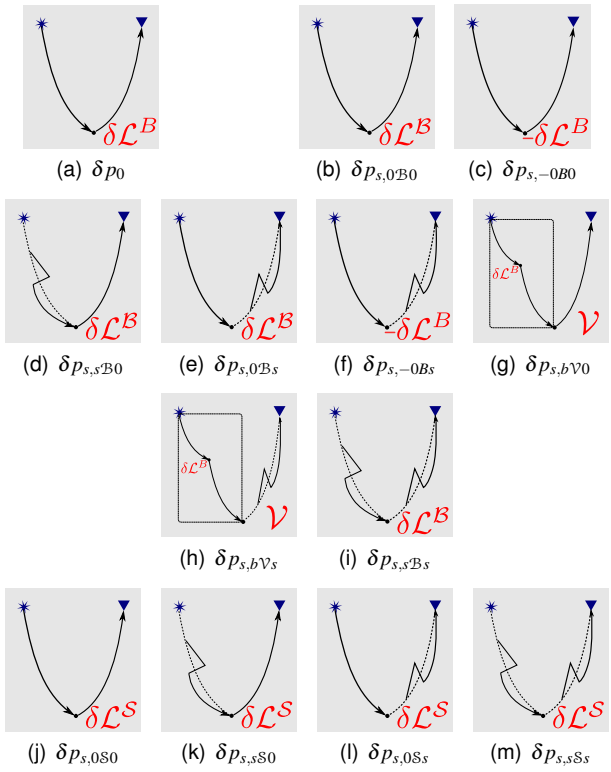

Figure 2: Physical interpretation of the subkernel contributions. Each one of the cartoons shows three elements: *source-side wavefield*; the *operator* applied to generate the secondary source; and the *receiver-side wavefield extrapolator*. Subcaptions indicate the name of the contribution with subscripts explained in the text.

with $i = 0\mathcal{B}0$, $0\mathcal{B}s$, $s\mathcal{B}0$, $s\mathcal{B}s$, $-0B0$, $-0Bs$, $b\mathcal{V}0$, $b\mathcal{V}s$, and $j = 0\mathcal{S}0$, $0\mathcal{S}s$, $s\mathcal{S}0$, and $s\mathcal{S}s$.

Under the separation into background and singular components proposed here, estimates of background and singular model perturbations can be evaluated individually by backprojecting the residuals. The perturbation estimates are given by the adjoint to equation (2). They are obtained from

$$\begin{bmatrix} \delta K^{\text{est}}_{B,0} + \sum_i \delta K^{\text{est}}_{B,i} \\ \sum_j \delta K^{\text{est}}_{S,j} \end{bmatrix} = \begin{bmatrix} U^\dagger & \sum_i U^\dagger_{B,i} \\ 0 & \sum_j U^\dagger_{S,j} \end{bmatrix} \begin{bmatrix} \widehat{\delta p_0} \\ \widehat{\delta p_s} \end{bmatrix}. \qquad (3)$$

The physical meaning of these estimates is the same as the one given by Tarantola (1984). At each point x of the model, they are the cross-correlation between the direct wavefield from source with the (once or twice) backpropagated residual from the receivers. for example, estimates $\delta K^{\text{est}}_{B,0\mathcal{B}s}$ explicitly reads

$$\delta K^{\text{est}}_{B,0\mathcal{B}s}(x) = \sum_s \sum_g \int d\omega\, \frac{-\omega^2}{K^2(x)}\, \overbrace{\widehat{p}^\dagger_0(x,\omega;x_s)}^{\text{direct wavefield}}\, \underbrace{\widehat{G}^\dagger_0(x,\omega;x_g)\widehat{\delta p}_s(x_g,\omega;x_s)}_{\text{back-propagation of } \widehat{\delta p}_s} \qquad (4)$$

To get the explicit expressions of the other sensitivity

kernels, one just needs to do the proper substitution of the wavefields and potentials.

Time-lapse survey as a FWI scattering problem

Both the baseline and monitor models are decomposed into a background and a singular part, where both parts of the baseline model are considered as known (background part: best smooth velocity model; singular part: reflector positions in the corresponding migrated image). The time-lapse change can be considered as perturbation to the singular or background parts.

If time-lapse change is considered a perturbation of the singular part, according to equation (2), the data difference between baseline and monitor is the scattered-wavefield residual and the model perturbation estimates are

$$\begin{bmatrix} \delta K_B^{\text{est}} \\ \delta K_S^{\text{est}} \end{bmatrix} = \begin{bmatrix} \sum_i \delta K_{B,i}^{\text{est}} \\ \sum_j \delta K_{S,j}^{\text{est}} \end{bmatrix} = \begin{bmatrix} \sum_i U_{B,i}^{\dagger} \\ \sum_j U_{S,j}^{\dagger} \end{bmatrix} \widehat{\delta p}_s. \quad (5)$$

Numerical experiments

To test our approach, we have set up two model sets with simple layered models (see Figure 3). The two baseline models are identical except for the deepest layer which in one of them is a strong reflector. The monitor models differ from the baseline models by a 5% velocity perturbation of 400 m width within the 4^{th} layer. The density was considered constant in all models (2200 kg/m^3). In

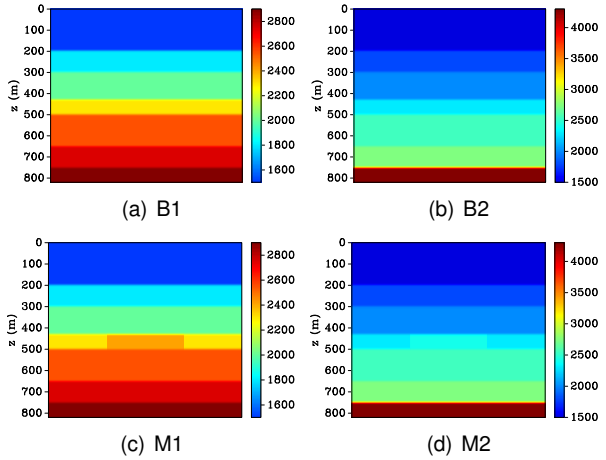

(a) B1 (b) B2

(c) M1 (d) M2

Figure 3: The baseline (a and b) and monitor (c and d) models for model sets 1 (a and c) and 2 (b and d).

this initial step of our study we consider that both the background and singular parts of the baseline velocity model are fully known.

The numerical experiments consisted of the following basic steps:

1. Wavefields were calculated in the baseline and monitor models as well as the smooth background models to determine the full, reference, and scattered true wavefield residuals for a given source.
2. These residuals were backpropagated once or twice – in subkernels of Figure 2(g) and 2(h) – from a given receiver by the proper extrapolator.
3. Each backpropagated wavefield residual was cross-correlated with the proper direct wavefield (full, reference, or scattered) from that given source.
4. Finally, the resulting wavefields were stacked over time (frequency), sources and receivers.

We performed non-simultaneous multiple-shots experiments. Source and receiver positions are marked by white stars and triangles, respectively, in the following figures.

Large offset surveys

In both sets of baseline/monitor models, we performed a 87-shots survey spread over a range of 2740 m spaced at 32 m.

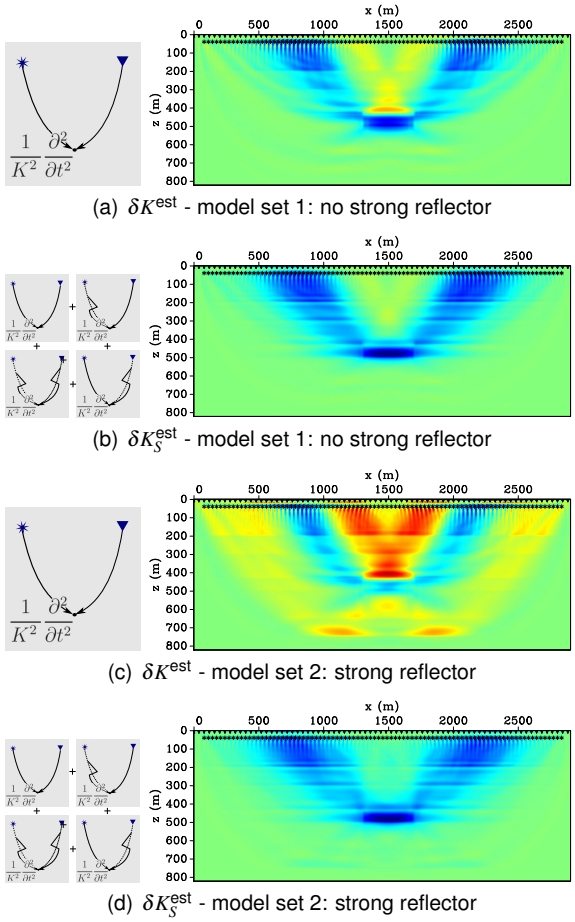

(a) δK^{est} - model set 1: no strong reflector

(b) δK_S^{est} - model set 1: no strong reflector

(c) δK^{est} - model set 2: strong reflector

(d) δK_S^{est} - model set 2: strong reflector

Figure 4: Estimates for the full and singular-part bulk-modulus perturbation.

In Figure 4 we show the estimates for the full and singular-part bulk-modulus perturbation for both model sets. Since the time-lapse change was considered a singular-part perturbation, all estimates should be similar. In Figure 4(a), we can see that in the absence of a strong reflector in the bottom of the model, the conventional sensitivity kernel gives a satisfactory estimate. By conventional sensitivity we the one that uses reference wavefields as source-side wavefield and receiver-side extrapolator. This was expected as we use large offset information to perform the

inversion. But this is not the case when a strong reflection event interferes with the single scattering assumption even when using a smooth background (Figure 4(a)).

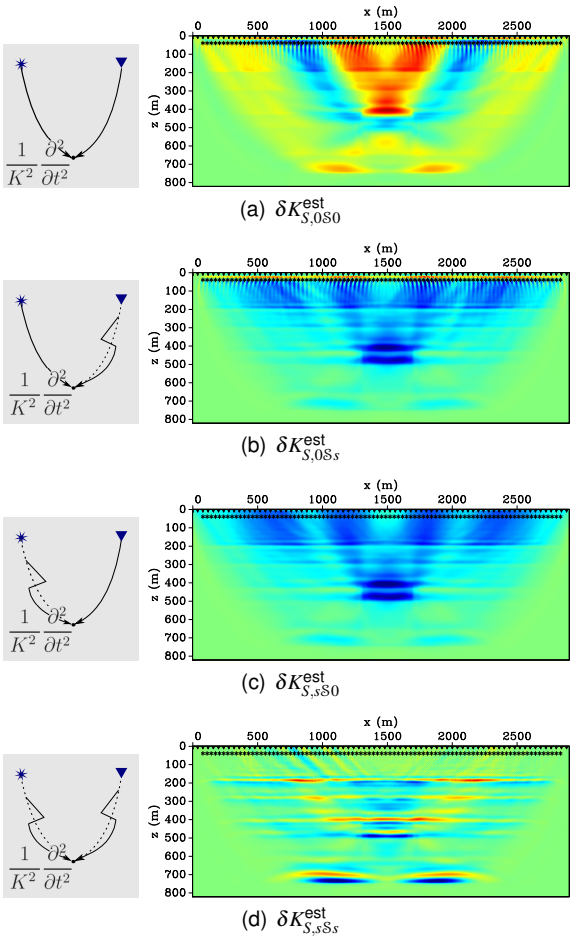

(a) $\delta K^{\text{est}}_{S,0S0}$

(b) $\delta K^{\text{est}}_{S,0Ss}$

(c) $\delta K^{\text{est}}_{S,sS0}$

(d) $\delta K^{\text{est}}_{S,sSs}$

Figure 5: Individual contributions to δK^{est}_S seen in Figure 4(d).

When multiple-scattering information is taken into account, this yields much better estimates. In Figure 5 we exhibit the individual contributions to δK^{est}_S seen in Figure 4(d). We can see more clearly that the superposition of the multiple-scattering contributions on the single-scattering estimate corrects the latter.

Narrow offset surveys

When inversion is done with enclosing, source and receiver arrays behave as in transmission tomography, which is known to recover very well the low-frequency information (see,e.g., Pratt, 1999; Brenders and Pratt, 2007). On the other hand, according to Zhu et al. (2009), when dealing with reflection/scattered data, narrower offsets (or reflection angles) may lead to fast-varying sensitivity kernels, in opposition to slow-varying ones in large-offset acquisitions. Fast-varying sensitivity kernels cause slower convergence of the inversion procedure.

To evaluate how a narrow-offset acquisition geometry affects the model reconstruction with our decomposed kernels, we next performed a 46-shots survey spread over a range of 904 m spaced at 20 m in both sets of baseline-monitor models. This experiment demonstrates that the self-illumination due to scattering gives better perturbation estimates.

Figures 6(a) and 7(a) depict the estimates for the two sets of models obtained with conventional sensitivity kernels. As expected, the figures display fast-varying estimates due to the narrow-offset illumination. But the message to be taken home is that these estimates are practically the same for both model sets. This shows that the reference-wavefield-based kernel does not exploit the information carried by the backscattered wavefield from the deep reflector.

Figure 6(b) shows the estimate obtained with the scattering-based sensitivity kernel for the set of models with no strong reflector. It shows that this kernel delivers almost no improvement compared with the conventional one (Figure 6(a)) due to the absence of the back-scattered information in this case.

On the other hand, in the strong reflector case, the multiple-scattered information improves the perturbation estimates giving a less varying and more delineated response (compare Figure 7(a) with 7(b)). This indicates that the multiple-scattering contribution perceives both the low- and high-frequency content of the perturbation.

Finally, comparing the singular-part perturbation estimate δK^{est}_S with its multiple-scattering contribution $\delta K^{\text{est}}_{S,sS0}$ (Figures 7(b) and 7(c)), we see that the latter contribution alone does a better job. The reason is that in this case the singularities, not the source array, act as sources of the source-side wavefield in the kernel. So to speak, the strong reflector is illuminating the time-lapse change from bottom to top.

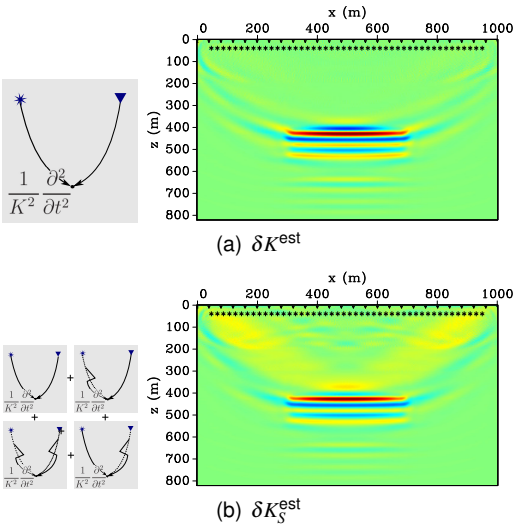

(a) δK^{est}

(b) δK^{est}_S

Figure 6: Estimates of the perturbation in the absence of strong reflector bellow the time-lapse change.

Summary and Conclusions

Considering time-lapse change as a perturbation on the singular part we circumvent the problem of separating the reference wavefield from the scattered which is subject to a parallel study.

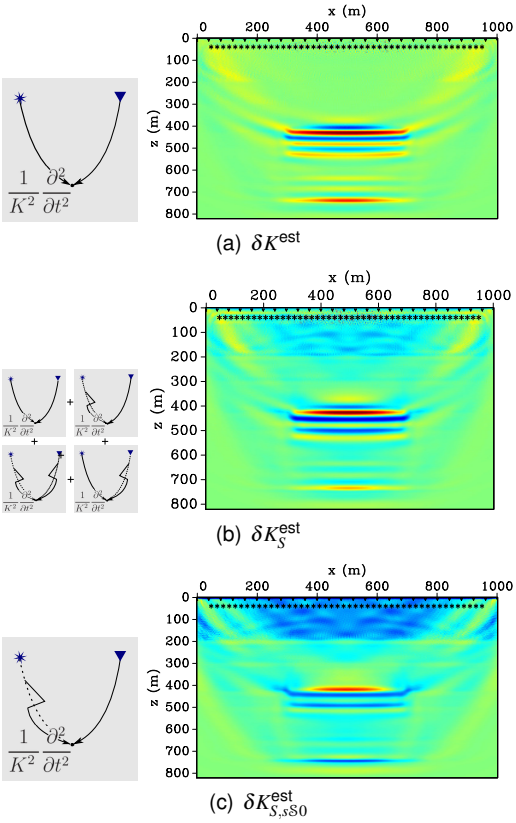

Figure 7: Estimates and multiple-scattering contribution of the perturbation in the presence of strong reflector bellow the time-lapse change.

Using the FWI differential method, if we consider the baseline model fully known, the data difference between baseline and monitor surveys is the residual to be minimized in order to obtain time-lapse change estimates using the baseline as starting model.

In the presence of a strong reflector bellow the time-lapse change, the use of the multiple-scattering-based sensitivity kernels gave better estimates in both large- and narrow-offset surveys compared to estimates obtained with the conventional sensitivity kernel. In the large-offset case, it was superior in handling the the backscattered information coming from the deep reflector which, otherwise, would give rise to spurious estimates. In the narrow-offset case, the scattering-based sensitivity kernels help to bring out the In other words, in some subkernels (e.g., $U_{S,s\mathcal{B}0}$) that has the scattered wavefield as source-side wavefields, the singularities/reflectors – origin of the scattered wavefield – act as source of illumination, improving/enlarging the espectral content of the estimate. low-frequency information carried by the back-scattered wavefield coming up from the deep reflector. In other words, for some subkernels (e.g., $U_{S,s\mathcal{B}0}$) the scattered wavefield acts as source-side wavefield. Then, the singularities or reflectors that originate the scattered wavefield act as source of illumination, enhancing the spectral content of the estimate.

Acknowledgments

This work was kindly supported by the Brazilian National Research Council CNPq as well as Petrobras, Schlumberger, and the sponsors of the Wave Inversion Technology (WIT) Consortium.

References

Asnaashari, A., R. Brossier, S. Garambois, F. Audebert, P. Thore, and J. Virieux, 2012, Time-lapse imaging using regularized FWI: a robustness study: SEG Technical Program Expanded Abstracts.

Brenders, A. J., and R. G. Pratt, 2007, Efficient waveform tomography for lithospheric imaging: implications for realistic, two-dimensional acquisition geometries and low-frequency data: Geophysical Journal International, **168**, 152–170.

Lumley, D. E., 2001, Time-lapse seismic reservoir monitoring: Geophysics, **66**, 50–53.

Macedo, D. L., I. Vasconcelos, and J. Schleicher, 2012, A Scattering-based Reparameterization of Sensitivity Kernels for Full-waveform Inversion: 74th EAGE Conference Tecnical Program Extended Abstracts.

———, 2013, Scattering-based sensitivity kernels for full-waveform inversion: taking advantage of medium self-illumination: SEG Workshop - Full Waveform Inversion: From Near Surface to Deep.

Plessix, R.-E., S. Michelet, H. Rynja, H. Kuehl, J. W. de Maag, and P. Hatchell, 2010, Some 3D applications of full waveform inversion: 72nd EAGE Conference Extended Abstracts.

Pratt, R. G., 1999, Seismic waveform inversion in the frequency domain, Part 1: Theory and verification in a physical scale model: Geophysics, **64**, 888–901.

Snieder, R., A. Grêt, H. Douma, and J. Scales, 2002, Coda wave interferometry for estimating nonlinear behavior in seismic velocity: Science, **295**, 2253.

Tarantola, A., 1984, Inversion of seismic reflection data in the acoustic approximation: Geophysics, **49**, 1259–1266.

Virieux, J., and S. Operto, 2009, An overview of full-waveform inversion in exploration geophysics: Geophysics, **74**, WCC1.

Watanabe, T., S. Shimizu, E. Asakawa, and T. Matsuoka, 2004, Differential waveform tomography for time-lapse crosswell seismic data with application to gas hydrate production monitoring: SEG Technical Program Expanded Abstracts, 1–4.

Zhu, H., Y. Luo, T. Nissen-Meyer, C. Morency, and J. Tromp, 2009, Elastic imaging and time-lapse migration based on adjoint methods: Geophysics, **74**, WCA167.